Draft version March 17, 2016
Preprint typeset using LaTeX style emulateapj v. 08/13/06

OBSERVATIONAL CONSTRAINTS ON THE ORBIT AND LOCATION OF PLANET NINE IN THE OUTER SOLAR SYSTEM

Michael E. Brown & Konstantin Batygin
Division of Geological and Planetary Sciences, California Institute of Technology, Pasadena, CA 91125
Draft version March 17, 2016

ABSTRACT

We use an extensive suite of numerical simulations to constrain the mass and orbit of Planet Nine, the recently proposed perturber in a distant eccentric orbit in the outer solar system. We compare our simulations to the observed population of aligned eccentric high semimajor axis Kuiper belt objects and determine which simulation parameters are statistically compatible with the observations. We find that only a narrow range of orbital elements can reproduce the observations. In particular, the combination of semimajor axis, eccentricity, and mass of Planet Nine strongly dictates the semimajor axis range of the orbital confinement of the distant eccentric Kuiper belt objects. Allowed orbits, which confine Kuiper belt objects with semimajor axis beyond 230 AU, have perihelia roughly between 200 and 350 AU, semimajor axes between 300 and 900 AU, and masses of approximately 10 Earth masses. Orbitally confined objects also generally have orbital planes similar to that of the planet, suggesting that the planet is inclined approximately 30 degrees to the ecliptic. We compare the allowed orbital positions and estimated brightness of Planet Nine to previous and ongoing surveys which would be sensitive to the planet's detection and use these surveys to rule out approximately two-thirds of the planet's orbit. Planet Nine is likely near aphelion with an approximate brightness of $22 < V < 25$. At opposition, its motion, mainly due to parallax, can easily be detected within 24 hours.

Subject headings:

1. INTRODUCTION

Since the time of the discovery of Sedna, it has been clear that a large perturbing mass either is or was present in the outer solar system at some time (Brown et al. 2004). With a perihelion distance of 76 AU, Sedna is essentially immune to direct interactions with the known planets, thus, unlike all other Kuiper belt object orbits, it cannot have been placed onto its orbit by perturbation from any of the known planets. Proposals for the perturber required to have created Sedna's orbit have included sibling stars in the sun's birth cluster (Brown et al. 2004; Brasser et al. 2006; Dukes & Krumholz 2012), a single passing star (Morbidelli & Levison 2004; Kenyon & Bromley 2004; Rickman et al. 2004) as well as a small former or extant planet in the outer solar system (Brown et al. 2004; Gladman & Chan 2006; Gomes et al. 2006). Progress on understanding the cause of Sedna's perturbed orbit, however, was not possible because of a lack of additional high perihelion objects.

With the discovery of 2010 GB174 (Chen et al. 2013) and 2012 VP113 (Trujillo & Sheppard 2014) – the second and third high perihelion Sedna-like objects – additional patterns began to emerge. Most importantly, Batygin & Brown (2016) point out that all well-determined orbits of Kuiper belt objects (KBOs) beyond Neptune with semimajor axis, a, larger than 230 AU approach perihelion within 94 degrees of longitude of each other. Moreover, these objects also share very nearly the same orbital plane, which is tilted an average of 22 degrees to the ecliptic. The combined probability of these two occurrences happening simply due to chance is less than 0.01%. Importantly, of all KBOs with $a > 100$ AU, the five with the largest perihelion distances are likewise confined to the same perihelion region and orbital plane.

Batygin & Brown (2016) show that a distant massive eccentric planet will cause clustering of the perihelion and orbital planes of distant Kuiper belt objects in the manner observed, and, additionally, will naturally lead to the creation of objects with high perihelion orbits like Sedna. Surprisingly, these clustered and high perihelion objects have orbits that are anti-aligned with the giant planet. That is, the clustered Kuiper belt objects come to perihelion 180 degrees away from the perihelion position of the planet. Despite chaotic evolution, the crossing orbits maintain long term stability by residing on a interconnected web of phase-protected mean motion resonances.

The distant eccentric perturber studied in Batygin & Brown (2016) – which we refer to as Planet Nine – modulates the perihelia of objects in the anti-aligned cluster and naturally creates objects like Sedna, in addition to the other high perihelion KBOs. Additionally, the existence of Planet Nine predicts a collection of high semimajor axis eccentric objects with inclinations essentially perpendicular to the rest of the solar system. Unexpectedly, this prediction is strongly supported by the collection of low perihelion Centaurs with perpendicular orbits whose origin had previously been mysterious (Gomes et al. 2015).

Here we make detailed comparisons between dynamical simulations that include the effects of Planet Nine, and solar system observations, to place constraints on the orbit and mass of the distant planetary perturber. We then discuss observational constraints on the detection of this distant giant planet and future prospects for its discovery.

Electronic address: mbrown@caltech.edu, kbatygin@gps.caltech.edu

2. CONSTRAINTS ON MASS, SEMIMAJOR AXIS, AND ECCENTRICITY

The inclined orbits of the aligned KBOs (and thus, presumably, of the distant planet) render ecliptic-referenced orbital angles awkward to work in (particularly when we consider the Centaurs with perpendicular orbits later). Accordingly, we re-cast the three ecliptic-referenced parameters – argument of perihelion, longitude of ascending node, and inclination – into simple descriptions of orbit in absolute position on the sky: the ecliptic longitude of the point in the sky where the object is at perihelion (which we call the "perihelion longitude", not to be confused with the standard orbital parameter called "longitude of perihelion" which, confusingly, does not actually measure the longitude of the perihelion except for zero inclination orbits), the latitude of the perihelion ("perihelion latitude"), and an angle which measures the projection of the orbit pole onto the plane of the sky ("pole angle" perhaps more easily pictured as the direction perpendicular to the motion of the object at perihelion).

Figure 1a shows the perihelion longitude and latitude as well as the pole angle for all objects with $q > 30$ and $a > 60$ AU and well-determined orbits. The six objects with $a > 230$ AU are highlighted in red. The clustering in perihelion location as well as pole angle is clearly visible. In Figure 1b we plot the perihelion longitude of all well constrained orbits in the Kuiper belt which have perihelia beyond the orbit of Neptune as a function of semimajor axis. The 6 objects with $a > 230$ AU cluster within 94 degrees of perihelion longitude. Batygin & Brown (2016) showed that this clustering, when combined with the clustering in pole angle, was unexpected at the 99.993% confidence level. The clustering is consistent with that expected from a giant planet whose perihelion is located 180 degrees in longitude away from the cluster, or an ecliptic longitude of 241 ± 15 degrees. A closer examination of Figure 1b makes clear a possible additional unlikely phenomenon. While KBOs with semimajor axes out to 100 AU appear randomly distributed in longitude, from 100 to 200 AU, 13 objects are loosely clustered within 223 degrees of each other. While this clustering is not as visually striking, the probability of such a loose clustering of 13 objects occurring in randomly distributed data is smaller than 5%. As will be seen, such a loose clustering of smaller semimajor axis objects can indeed be explained as a consequence of some orbital configurations of a Planet Nine.

To understand how these observations constrain the mass and orbit of Planet Nine, we performed a suite of evolutionary numerical integrations. Specifically, we initialized a planar, axisymmetric disk consisting of 400 eccentric planetesimals, that uniformly spanned semimajor axis and perihelion, q, distance ranges of $a = 150 - 550$ AU and $q = 30 - 50$ AU, respectively. The planetesimal population (treated as test particles) was evolved for 4 Gyr under the gravitational influence of the known giant planets, as well as Planet Nine.

Perturbations due to Planet Nine and Neptune were accounted for in a direct N-body fashion, while the secular effects of the remaining giant planets were modeled as a suitably enhanced quadrupolar field of the Sun. As shown in Batygin & Brown (2016), such a numerical setup successfully captures the relevant dynamical phenomena, at a substantially reduced computational cost.

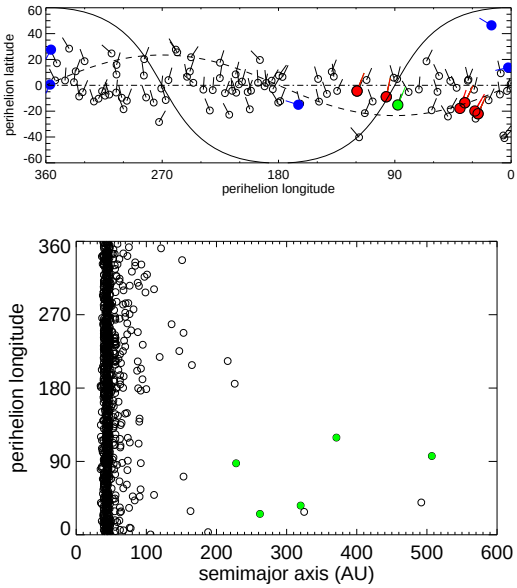

FIG. 1.— Orbital parameters of distant Kuiper belt objects. (a) The standard orbital parameters argument of perihelion, longitude of ascending node, and inclination can be transformed into non-standard, but more readily interpretable ecliptic longitude and latitude of the point where the object comes to perihelion and an angle which is a projection of the orbits pole position on the sky. In this representation, the collection of all objects with $q > 30$ and $a > 60$ AU is shown. The six objects with the highest semimajor axis are highlighted in red. The KBO 2000 CR105, which has the seventh largest semimajor axis and has an elevated perihelion of 44 AU, is shown in green. The blue points are all of the object with $a > 230$ AU and $i > 50$ degrees. All of these objects are Centaurs with perihelia inside of 15 AU. (b) A plot of the semimajor axis versus the ecliptic longitude at which the object comes to perihelion for all KBOs with well determined orbits and with $q > 30$ AU shows that the six KBOs with the largest semimajor axes are clustered within 94 degrees of each other. The green points additionally highlight all objects with $a > 100$ AU and $q > 42$ AU, showing that these objects, too, are similarly clustered. The weaker potential clustering of objects ∼180 degrees away is also evident between 100 and 200 AU.

In these integrations we varied the semimajor axis and eccentricity of Planet Nine from $a_9 = 200 - 1000$ AU and $e_9 = 0.1 - 0.9$ in increments of $\Delta a_9 = 100$ AU and $\Delta e_9 = 0.1$ (here, and subsequently, the 9 subscript refers to the orbital parameters of Planet Nine, while unsubscripted orbital parameters refer to the test particles). The $a_9 - e_9$ grids of synthetic scattered disks were constructed for Planet Nine masses of $m_9 = 0.1$, 1, and 10 M_e (earth masses), totaling a suite of 192 simulated systems. All calculations were performed using the `mercury6` N-body integration software package (Chambers 1999), employing the hybrid symplectic-Bulirsch-Stoer algorithm with a timestep equal to a tenth of Neptune's orbital period.

We assess the success of each simulation with a simple metric. We collect the orbital elements of all remnant objects at each 0.1 Myr output time step from 3 to 4 Gyr after the start of the simulation (in order to assure that the objects we are considering are stable over

at least most of the age of the solar system), and we restrict ourselves to objects with instantaneous perihelion $q < 80$ AU (to restrict ourselves to objects which are most likely to be observable). In this fashion we are examining stream functions of orbital elements which fit into an observable range of parameter space, rather than examining individual objects at a single time step. This approach is used in all subsequent discussions of simulations below. We then select 13 objects at random in the $a = [100, 200]$ AU range and 6 objects at random in the $a = [230, 600]$ AU range and calculate the smallest angles that can be used to confine the two populations. We perform this random selection 1000 times and calculate the joint probability that, like the real data, the 13 objects in $a = [100, 200]$AU range are confined within 223 degrees and the 6 objects $a = [230 - 600]$ AU range are confined within 94 degrees. Additionally, we examine whether *any* objects exist in the range $a = [200, 300]$ AU, as many simulations remove all objects in this range. We assign these simulations a probability of zero. This probability calculation has the advantage that it is agnostic as to whether or not our observations of clustering are significant or even physically relevant. It simply calculates the probability that a given simulation could reproduce some of the apparent features of the real data, even if by chance. A small number of simulations which do well in our simplistic metric nonetheless give results so unlike the solar system observations that we manually assign them zero probability.

Figures 2 and 3 show grids of probabilities for the 10 and 1 M_e simulations (the 0.1 M_e simulations had no appreciable effect on the objects). The probabilities should be taken as more qualitative than quantitative, as these simulations are exploratory and attempt to cover large ranges of phase space by including a limited number of particles per simulation and excluding three dimensional effects. Nonetheless, the overall trends are clear. All of the 1 M_e cases can be ruled out at greater than the 98% confidence level. The only simulation which fits the outer part of the Kuiper belt even slightly well, with Planet Nine at $a_9 = 200$ AU and $e_9 = 0.7$ would have a perihelion of $q_9 = 60$ AU, which would be likely to do significant damage to the largely undisturbed cold classical Kuiper belt which we did not include in our simulations. We thus conclude that a mass as low as 1 M_e is infeasible.

The 10 M_e simulations produce a wide range of acceptable results (Figure 2). In general, all simulations which cannot be excluded at at the 99% confidence level fall with a range of $a_9 = [300, 900]$ AU and $q_9 \sim [200, 350]$ AU. The acceptable q_9 range is greater at smaller semimajor axis. The acceptable simulations can be roughly described as fitting within a triangular region of phase space defined by [a_9, e_9] corners of [300 AU, 0.5], [300 AU, 0.1], and [900 AU, 0.8]. The best fit simulations are along the $q_9 \sim 200$ AU line with the middle range of semimajor axis.

In Figure 4 we show, as an example, the Planet Nine-centered perihelion longitudes as a function of a of all objects that have $q < 80$ AU and which have survived at least 3 Gyr, for the case of $a_9 = 500$ AU and $e_9 = 0.6$, one of the highest probability simulations. Objects anti-aligned with the planet have a longitude of 180 degrees in this simulation, while those aligned will be at 0 degrees longitude. This simulation shows the major effects that

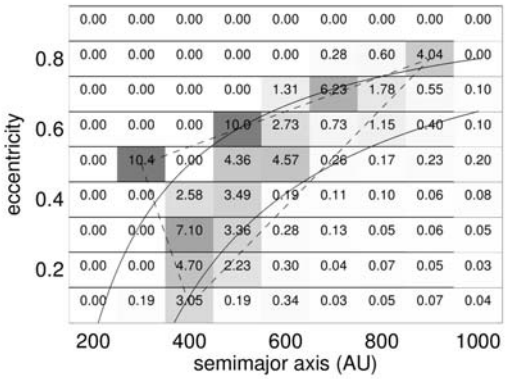

FIG. 2.— Only a limited set of simulated 10 M_e Planet Nine orbits provide an adequate fit to the known orbits of the distant KBOs. For each semimajor axis - eccentricity combination, we calculate the probability that 6 objects selected at random with $230 < a < 600$, $q < 80$ AU and at times $t > 3$ Gyr are clustered within 94 degrees of each other combined with the probability that 13 objects randomly selected with $100 < a < 200$ and $q < 80$ AU. Acceptable simulations (with a probability of greater than 1%) occupy a roughly triangular region of a-e space (show in dashed lines) with perihelion distances between 200 and 350 AU (shown in solid lines).

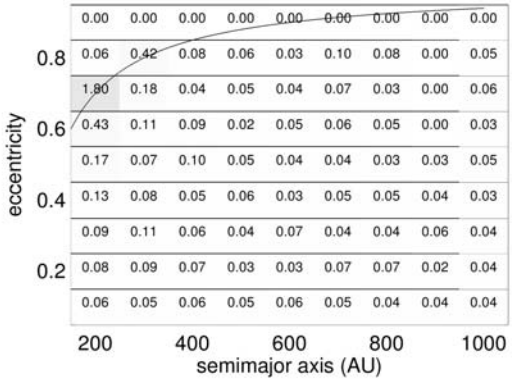

FIG. 3.— For a 1 M_e Planet Nine with $a_9 = 200$ AU and $e_9 = 0.7$ a marginal fit appears acceptable, but detailed examination of the simulation shows that the results diverge greatly from the solar system. Most other combinations of orbital parameters show little effect on the Kuiper belt.

we have previously identified in the real data. Inside of 100 AU little perturbation is visible. From 200 to 600 AU the longitudes are confined around 180 degrees, that is, they are anti-aligned with Planet Nine. And from 100 to 200 AU there is a slight tendency for a broad cluster centered on the longitude of the planet.

As a counter example, Figure 5 shows a simulation with $a_9 = 700$ AU and $e_9 = 0.3$ which depicts many of the same general phenomena, but these phenomena do not develop until larger semimajor axes. For example, the anti-alignment does not begin until 400 AU, while a broad aligned cluster can be seen from about 300 to 400 AU. Even with the crudeness of these simulations these basic effects are clear. The semimajor axis at which anti-alignment begins and the range where broad confinement is evident are strong indicators of the combination of semimajor axis and the eccentricity of Planet Nine.

We have not yet performed simulations with higher mass planets, so the upper limit to the mass is not yet known. Further simulations are required to constrain

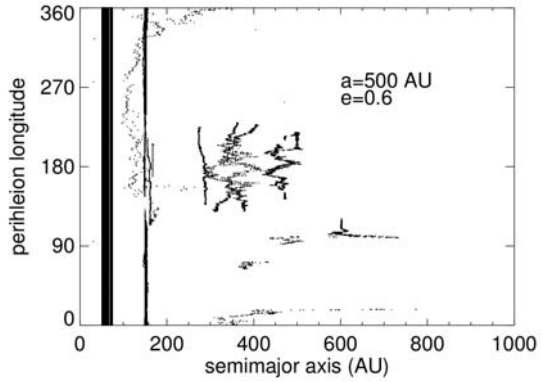

FIG. 4.— One of the successful simulations showing the orbital evolution of all objects with $q < 80$ AU at times $t > 3$ Gyr. A collection of resonant stable high semimajor axis objects anti-aligned with Planet Nine (centered at Δ longitude of 180 degrees) appears beyond 200 AU, while from 100-200 AU there is a slight preference for aligned orbits.

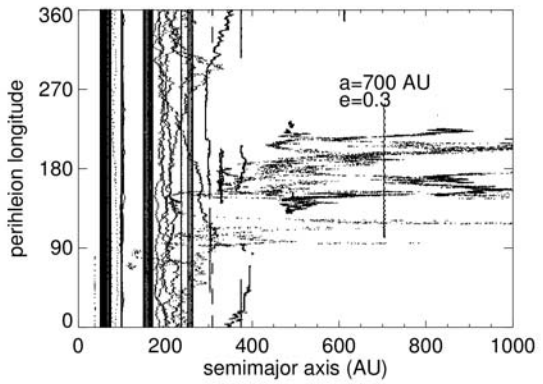

FIG. 5.— A low probability simulation. Clear anti-alignment does not develop until beyond 400 AU, while aligned orbits appear only from approximately 300 to 400 AU.

the mass of Planet Nine to a greater degree of accuracy, though, as we show below, current imaging survey constraints rule out masses higher than about 20 M_e.

3. CONSTRAINTS ON INCLINATION AND ARGUMENT OF PERIHELION

The planar simulations provide no constraints on inclination, i_9, argument of perihelion ω_9, or longitude of ascending node, Ω_9, of Planet Nine. To examine the effects of these orbital elements on the Kuiper belt, we perform a second, fully three dimensional suite of simulations. In these simulations we fix the semimajor axis and eccentricity to be 700 AU and 0.6, respectively, values which are within our acceptable range of parameter space. The inclination dynamics are unlikely to be unique to the specific values of a_9 and e_9, so we deem these simulations to be representative. We allow the inclination of Planet Nine to take values of $i_9 = 1$, 10, 20, 30, 60, 90, 120, and 150 degrees.

Unlike the planar suite of calculations, here we initialize the planetesimals in a state characterized by an anti-aligned longitude of perihelion with respect to that of the planet. The starting values of planetesimals' longitudes of ascending node, on the other hand, are taken to be random. As demonstrated by Batygin & Brown (2016), dynamical sculpting of such a planetesimal population yields a configuration where long-term stable objects have longitudes of ascending node roughly equal to that of Planet Nine. In turn, this ties together ω_9 and Ω_9 through a fixed longitude of perihelion (which is the sum of these parameters).

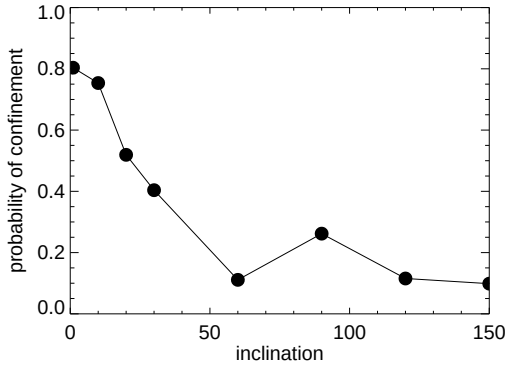

FIG. 6.— For simulations with $a_9 = 700$AU and $e_9 = .6$, the probability of confinement of 6 randomly selected objects with $300 < a < 700$ and $q < 80$ AU varies strongly with inclination of the planet.

Upon examination of these simulations, we find that efficiency of confinement of the distant population drops dramatically with increased inclination of Planet Nine. To quantify this efficiency, we sample each simulation 1000 times, picking 6 random objects from the sample of all objects in the range $a = [300, 700]$ AU (as previously shown, these $a_9 = 700$ AU simulations do not begin strong perihelion confinement until $a \sim 300$ AU; as we are more interested in understanding the cluster than in specifically simulating our data at this point we increase our semimajor axis range of interest). As before we restrict ourselves to time steps after 3 Gyr in which an object's orbit elements have $q < 80$ AU, and we add the constraint that $i < 50$ degrees, to again account for observability biases. We calculate the fraction of times that the 6 randomly selected objects are clustered within 94 degrees (Figure 6). The confinement efficiency drops smoothly until, at an inclination of 60 degrees and higher, it scatters around 20%. These results suggest, but do not demand, that Planet Nine has only a modest inclination.

One of the striking characteristics of the 6 aligned distant Kuiper belt objects is the large value of and tight confinement in the pole angle (22 ± 6 degrees; Figure 1). In examining the simulations that exhibit good confinement in longitude, we note that the polar angles of the simulated orbits are approximately perpendicular to the plane of Planet Nine, particularly for objects which come to perihelion in the plane of the planet. The implication of this phenomenon is that a pole angle of 22 degrees suggests a minimum planet inclination of approximately 22 degrees, and an orbital plane (which is controlled by Ω_9) similar to the plane of the observed objects. To quantify this observation, we plot the median pole angle of our simulation objects which meet the criteria described above and which have perihelion latitudes between -25 and 0 degrees like the real distant objects. We restrict ourselves to objects with perihelia south of the ecliptic both because the observed objects all have perihelia south of the ecliptic and also because we want to avoid any bias that would occur by a loss of

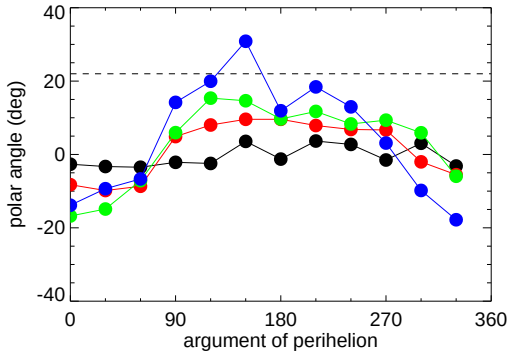

FIG. 7.— For the inclined simulations, the average polar angle of anti-aligned orbits varies systematically with ω_9. The average polar angle of the six most distant objects is 22 degrees, shown as the dashed line. For simulations with high probability of confinement ($i_9 < 60$ degrees), the average polar angle only reaches values as high as 22 degrees for $\imath_9 = 30$ degrees and ω_9=150 degrees. The black, red, green, and blue points correspond to the i_9=1, 10, 20, and 30 degree simulations, respectively.

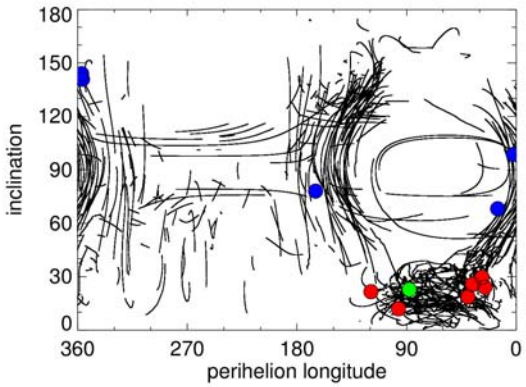

FIG. 8.— For simulations with $a_9 = 700$ AU, $e_9 = 0.6$, and $i_9 = 30$ deg, examination of all objects with $300 < a < 700$ AU and $q < 80$ Au shows a low inclination population anti-aligned with Planet Nine and a high inclination population on either side of the anti-aligned population. The colored points are the same as in Figure 1a, with the blue points showing that the highly inclined large semimajor axis Centaurs are closely aligned with the predicted high inclination locations.

observed objects north of the ecliptic due to the proximity of the galactic plane close to the perihelion positions. It is currently unclear whether the lack of clustered objects with perihelia north of the ecliptic is a dynamical effect or an observational bias. Figure 7 shows this mean polar angle as a function of argument of perihelion of Planet Nine. The maximum median polar angle occurs for $\omega_9 \sim 150$ degrees, a configuration where the plane of the planet passes through the perihelion positions of the objects, and that maximum is approximately equal to the inclination of the orbit, confirming our observation that the clustered objects are along the same orbit plane as the planet.

Based on the confinement probability and the large average pole angle of the real objects, we can infer that the inclination of Planet Nine is greater than ∼22 degrees and less than the inclination at which confinement becomes improbable, which, based on an interpolation of the data from Figure 5, occurs approximately around 40 degrees. For inclinations of ∼22 degrees, ω must be quite close to 150 degrees. For inclinations of 30 degrees, the allowable range for the argument of perihelion appears to be $\omega_9 \sim 120 - 160$ degrees.

While this analysis yields useful constraints, we quantify these results further by again sampling each of the simulations 1000 times and determining the probability of 6 randomly selected objects (300 AU $< a <$ 700 AU, $q <$ 80 AU, $i <$ 50 degrees, survival time greater than 3 Gyr, and perihelion latitude between -25 and 0 degrees) having perihelion longitudes clustered with 94 degrees and having an average polar angle greater than 20 degrees with an RMS spread of less than 6.2 degrees. Almost all simulations can be ruled out at greater than the 99% confidence level. The only simulations which cannot are, unsurprisingly, those with inclination of 30 degrees and argument of perihelion of 150 – which is the single best fit – and 120 degrees and, additionally, a few other seemingly random combinations of $[i_9, \omega_9]$: [90, 60], [150, 0], [150, 210], and [150, 330], all in units of degrees. We examine all of these cases in detail below.

One strong prediction of the existence of a giant planet in the outer solar system is that it will cause Kozai-Lidov oscillations which will drive modest inclination objects onto high inclination perpendicular and even retrograde orbits and then back again. This effect can be seen, for example, in Figure 8, where we plot the evolution of perihelion longitude versus inclination for the simulations with 30 degree inclination (again, restricting ourselves to 300> a >700 AU, $q < 80$ and $t > 3$ Gyr; note that argument of perihelion of Planet Nine has no substantive effect on this plot, so we plot all arguments together). The five known objects in the outer solar system with $a > 200$ AU and $i > 50$ deg are also shown. The simulations reproduce their perihelion longitudes and inclinations well, although they are all on the outer edge of the predicted clustering regions. An important caveat to note, however, is that the five high inclination objects are all Centaurs with $8 < q < 15$ AU. The high inclinations of these objects mean that they penetrate the giant planet region much more easily and so can maintain their alignments much more easily than lower inclination Centaurs. Our simulations remove all objects inside 20 AU, so we have not explored the dynamics interior to Uranus, but we note a systematic trend where objects with smaller perihelion distances move to the outer edge of the clustering regions, just like the real low perihelion objects appear to be. Clearly, simulations including all of the giant planets which allow us to study these high semimajor axis Centaurs are critical.

The perihelion locations of the perpendicular high semimajor axis Centaurs effectively rule out the possible higher inclination orbits for Planet Nine. The $i_9 = 90$ and $i_9 = 150$ degrees cases do create high inclination objects, but their perihelia are sporadically distributed across the sky (Figure 9). We conclude that, of our simulated parameters, only the $i_9 = 30, \omega_9 = 150$ degrees and $i_9 = 30, \omega_9 = 120$ degrees are viable.

In order to complete our analysis in a tractable amount of time, each of the simulations used to explore parameter space above was limited in either dimensionality, number of particles, or in the range of starting parameter of the particles. In order to check that these limitations did not influence the overall results, we perform a final fully three dimensional simulation with a large number of particles with randomly chosen starting angles. We

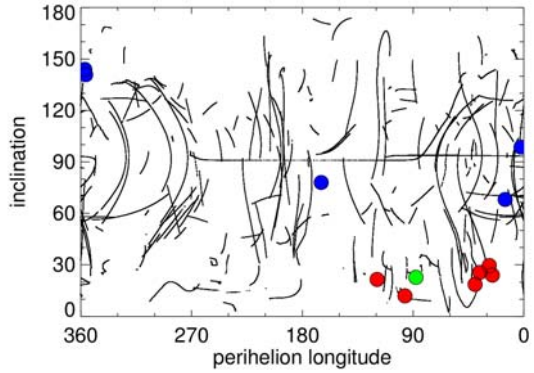

FIG. 9.— The simulations with $i_9 = 150$ degrees produce little confinement of either the low or high inclination population.

choose to simulate Planet Nine with a mass of 10 M_e, $a_9 = 700$, $e_9 = 0.6$, $i_9 = 30$ degrees, $\omega_9 = 0$ degrees, and $\Omega_9 = 0$ degrees (note that the planet processes over the 4 billion years of the integrations, but at this large semimajor axis the precession in ω_9 is only about 30 degrees during the entire period, so we ignore this effect). These full simulations reproduce all of the relevant effects of the more limited simulations, giving confidence to our simulation results.

4. SKY POSITION

Based on comparison to our suite of simulations, we estimate that the orbital elements of Planet Nine are as follows. The semimajor axis and eccentricity are within a triangle bounded by the [a_9,e_9] sides of [300 AU, 0.5], [300 AU, 0.1], and [900 AU, 0.8]; the inclination is between approximately $22 < i_9 < 40$ degrees, and the argument of perihelion is between $120 < \omega_9 < 160$ degrees. We fix the perihelion longitude at 241±15 degrees. While these choices of parameter ranges have been justified in the analysis of the simulations above, they cannot be considered a statistically rigorous exploration of parameter space. Indeed, any attempt at such statistical rigor is not yet warranted: substantial uncertainty comes not from the statistics of the objects themselves, but from the currently small number of simulations in the best fit region of parameter space. Clearly, significantly more simulation is critical for a better assessment of the path of Planet Nine across the sky.

The last parameter we consider is the mass of Planet Nine, which we assume is in the range of 5 to 20 M_e. To transform this mass into an expected brightness requires assumptions of both radius (and thus composition) and albedo (and thus surface composition), neither of which is constrained by any of our observations. Nonetheless, we note that many known exoplanets exist in this mass range, and they are thought to contain substantial gaseous atmospheres (Rogers 2015). Weiss & Marcy (2014) find a best-fit mass-radius relationship of $(R/R_e) = 0.34\,(M/M_e)^{1.08}$, which yields a radius of approximately 4 R_e for our nominal mass estimate and a range of 2 to 9 R_e for our full range. We note however, that compositional differences, as well as variable irradiation levels can introduce substantial scatter into the data (Batygin & Stevenson 2013). For albedo, we make the plausible assumption that Planet Nine will be an ice giant like Uranus or Neptune, with a similar

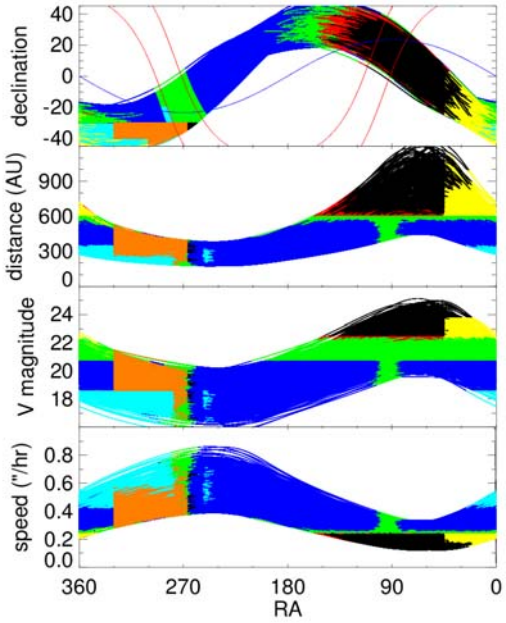

FIG. 10.— Using all constraints on the orbital and physical parameters of Planet Nine, we can predict the location, distance, brightness, and speed of the planet throughout its orbit. Regions within 10 degrees of the galactic plane are outlined in red, and the ecliptic plane is sown in blue. The colored portions show regions where Planet Nine would have been or should be detected by previous or ongoing surveys. Pink shows WISE limits. Light blue shows limits from the CRTS reanalysis, yellow shows Dark Energy Survey limits and covered, dark blue shows Pan-STARRS transient analysis limits, green shows Pan-STARRS moving object analysis current limits, and red shows Pan-STARRS expected limits. Orange shows the region exclusively ruled out by lack of observed perturbation to Saturn (Fienga et al. 2016) The black regions show regions of phase space where Planet Nine could not have been or will not be detected in previous or currently planned surveys.

atmospheric composition and structure, and albedo of ∼0.3.

We now use our estimated orbital parameters to predict the orbital path of Planet Nine across the sky. We carry out a simple Monte Carlo analysis selecting uniformly across all of the parameter ranges. Figure 10 shows the sky location, heliocentric distance, magnitude, and sky motion at opposition for our suite of predicted orbits. For the calculated V magnitude, we only consider planets as large as 4 R_e. As will be seen, a much larger planet can be ruled out over nearly its entire range.

5. CURRENT OBSERVATIONAL CONSTRAINTS

While most wide field surveys of the Kuiper belt have not been sensitive to sky motions smaller than about 1 arcsecond per hour (Millis et al. 2002; Brown 2008; Petit et al. 2011, i.e.), a few surveys have had the sensitivity and cadence to have potentially detected Planet Nine at some point in its orbit. We discuss all such surveys below.

5.1. *WISE*

The WISE spacecraft surveyed the entire sky twice in its 3.4 and 4.6 μm (W1 and W2) bands, allowing Luhman (2014) to rule out Saturn-sized planets – which have substantial enhanced short wavelength emission ow-

ing to emission from internal heat – out to a distance of ∼30,000 AU. A 10 M_e planet, however, would not be expected to have this enhanced short wavelength emission. For example, ISO detected nothing but reflected sunlight from Neptune from 2.5 to 5 μm (Burgdorf et al. 2003), with an average flux of about 5 mJy. The Luhman (2014) W1 limit corresponds to approximately 0.2 mJy, which suggests that Neptune itself could only be detected to ∼70 AU. As a confirmation, we examined the catalog of WISE single-source detections of Neptune itself. Neptune is detected 16 times with a signal-to-noise (S/N) of approximately 50 in the W1 band. Assuming that all of those images are coadded, Neptune could be detected with a S/N of 10 only to ∼63 AU, consistent with our estimate above. The Luhman (2014) results thus provide no constraints on the position or existence of Planet Nine.

5.2. *Catalina real time transient survey*

While near earth object searches are performed at cadences poorly matched to the detection of objects in the outer solar system, they cover the sky multiple times in a year, allowing the possibility of detecting objects by their weekly or monthly motion. In Brown et al. (2015), we performed such an analysis from the Catalina real time transient survey (CRTS)(Drake et al. 2009), which itself repurposed the Catalina Sky Survey near earth asteroid search into a transient survey. We collected all one-time transients over an 8 year period, that is, all instances in which an object was detected at a spot in the sky only once, and attempted to fit all combinations of 4 or more detections to Keplerian orbits. The Keplerian filter is strong. From $\sim 10^{19}$ potential combinations, we narrowed the detections down to eight known Kuiper belt objects and zero false positives. Every bright Kuiper belt object in the survey fields was detected, often dozens of times. The survey was determined to be essentially 100% complete to $V \sim 19.1$ in the north and $V \sim 18.6$ in the south. For some of the smaller potential values for semimajor axis and larger values of planetary radius, for example, Planet Nine would have been visible to this survey over a substantial portion of its orbit, though it was not detected.

5.3. *The Pan-STARRS 1 Survey*

The Pan-STARRS 1 telescope has surveyed large amounts of sky multiple times to moderate depths at declinations greater than -30 degrees. We consider the analysis of the data in two stages.

The Pan-STARRS Survey for Transients. Like the earlier, CRTS, the Pan-STARRS Survey for Transients (PST) (Smartt et al. 2014) quickly disseminates detections of transients sources detected in the sky. We have performed a similar analysis on the reported PST data, searching for viable Keplerian orbits. No series of transients can be found which fit an outer solar system body on any bound Keplerian orbit. Typical transient depths reached are $g = 21.0$, and based on the collection of reported transients, the survey appears to efficiently cover the sky north of -30 declination and at galactic latitudes greater than about 10 degrees. This survey rules out much of the sky within about 45 degrees of the predicted perihelion point, with the exception of the region near the galactic plane.

The Pan-STARRS Outer Solar System Key Project. A survey for objects in the outer solar system was one of the initial goals of the Pan-STARRS survey. Holman et al. (2015) have now completed a preliminary analysis of the survey data and report no detections out to 600 AU. While detailed sensitivity studies have yet to be completed, it is estimated that the survey is complete to approximately $r \sim 22.5$, though limits in the galactic plane are worse. An extended analysis is currently underway which will have the same brightness limits, but will remove the artificial restriction to objects closer than 600 AU (Holman, private communication). If these sensitivity estimates are correct, the Pan-STARRS 1 moving object survey has or will rule out a substantial fraction of the non-aphelion sky.

5.4. *The Dark Energy Survey*

The Dark Energy Survey (DES) is performing the largest deep southern hemisphere survey to date. Some of the DES region covers the orbital path of Planet Nine (indeed one of the 6 cluster objects, 2013 RF98, was detected in the DES). While cadences are not designed for ease of outer solar system detection, it is clear that the data will be sensitive to Planet Nine if it is in the survey area. The DES team estimates a Planet Nine detection limit of $r \sim 23.8$. (Gerdes, private communication).

5.5. *Additional surveys*

Additional surveys covering wide areas of the sky have been performed, but in all cases they are insensitive to the slow expected speeds of Planet Nine, they have too low of a survey efficiency to consider the region effectively surveyed, or they cover little or none of the region of the predicted orbital path. The large community surveys which are concentrating on specific areas of the sky, such as the VISTA surveys in the southern hemisphere and the Subaru Hyper-SuprimeCam survey along the celestial equator unfortunately do not overlap with the required search region.

In the future, the Large-Scale Synoptic Telescope is expected to survey much of the sky observable from its Chilean site to a single-visit depth of approximately $r \sim 24.5$ magnitude. The current survey strategy does not include visits to fields as far north as those at the extremes of the predicted Planet Nine orbital path, but if Planet Nine has not yet been found by the expected start of the LSST survey operations in 2023, a simple extension could quickly rule out nearly all but the faintest and most distant Planet Nine predictions.

At its most distant predicted locations, Planet Nine is faint and in the northern hemisphere. Subaru Hyper-Suprime Cam will be the instrument of choice for detecting the planet at these locations. We began a survey of these regions in the fall of 2015 and will attempt to cover all of the predicted orbital path.

5.6. *Additional constraints:*

Fienga et al. (2016) perform full fits to the locations of all planets and nearly 300 asteroids observed from ancient times to the present with and without a 10 M_e Planet Nine at various positions along an orbit with $a_9 = 700$ AU and e_9=0.6, consistent with the nominal orbit suggested in Batygin & Brown (2016). They find

that the strongest constraint on the existence of Planet Nine comes from the very precise measurements of the distance to Saturn as measured by the Cassini spacecraft over the past decade. They strongly rule out a 10 M_e Planet Nine closer than ∼400 AU over the range of Right Ascension of $RA_9 > 266$, $RA_9 < 2$ deg. When Planet Nine is beyond 600 AU, RA_9=[31,160] deg for this orbit, they can detect no difference between Saturn's position with and without Planet Nine. At intermediate distances, the signal from Planet Nine is difficult to disentangle from systematic effects. At two locations, RA_9=197 and RA_9=33 deg, the position of Saturn is slightly better explained with the addition of Planet Nine, but with two such minima, we conservatively take this fit to be indicative of the level of the systematic errors in the analysis. While Fienga et al. (2016) only fit the single nominal orbit, we estimate the range of orbits that they could have ruled out by noting that the ratio of the expected Planet Nine signal compared to the approximate level of the systematic noise is > 5 over most of the ruled out region, so we consider any planet with 20% of the tidal effect of the nominal Planet Nine to be ruled out. This constraint effectively rules out a small otherwise unobserved region in the southern hemisphere.

A recent paper (Malhotra et al. 2016) makes no attempt to explain spatial alignments, but instead attempts to simplistically look for mean-motion commensurabilities in the distant KBOs, in hopes of being able to constrain both a_9 and the location of Planet Nine within its orbit. Specifically they assume that the four most distant KBOs are in N:1 and N:2 resonances, and examine the implications for Planet Nine. Such an approach could, in principle, work in the circular restricted three-body problem, but, as shown in (Batygin & Brown 2016), highly elliptical orbits are required to explain the spatial confinement of the orbits, and no specific resonances dominate the disturbing function in this elliptical problem. Indeed, no particular preference for type of critical angle or even resonance order can be identified in the dynamical simulations shown here. Rather, the crossing orbits evolve chaotically but maintain long term stability by residing on a interconnected web of phase-protected mean motion resonances. The assumption of simple low order resonance is thus unlikely to be justified. Not surprisingly, the Planet Nine orbits produced by these assumptions do not produce the spatial confinements of the KBOs that are observed. Thus, it appears that no useful constraint on the orbit or position can be drawn from this method.

5.7. *Joint constraints*

In Figure 10 we show the regions of the potential orbits of Planet Nine that have been ruled out by the above constraints (or, in the case of the ongoing DES, where the planet might still be found by the survey). The existence of Planet Nine can be ruled out over about two thirds of its orbit. One tiny region in the southern hemisphere galactic plane remains uncovered by any existing surveys, but the probability of finding Planet Nine in such a small location right at perihelion is small. The vast majority of the orbital region in which Planet Nine could be located is beyond about 600 AU and within about 60 degrees of its aphelion position. For the eccentric orbits considered here, Planet Nine spends greater than half of its time at these distances, so finding it currently at these locations near aphelion would be expected.

At its most distant possible location, a 2 R_e Planet Nine is approximately $V = 25$. A 9 R_e Planet Nine, which is our estimated size for a 20 M_e object, would be 3.3 magnitudes brighter, for a faintest magnitude of $V = 21.7$. Such a bright object can already be ruled out at all points in its orbit, including the northern galactic plane. We thus consider 9 R_e an upper limit to the size and thus approximately 20 M_e an upper limit to the mass of Planet Nine (with the caveat that the mass-radius relationship remains uncertain).

6. CONCLUSIONS

The existence of a distant massive perturber in the outer solar system – Planet Nine – explains several hitherto unconnected observations about the outer solar system, including the orbital alignment of the most distant Kuiper belt objects, the existence of high perihelion objects like Sedna, and the presence of perpendicular high semimajor axis Centaurs. These specific observations have been compared to suites of numerical integrations in order to constrain possible parameters of Planet Nine. The current constraints must be considered preliminary: our orbital simulations needed to cover substantial regions of potential phase space, and so were, of necessity, sparsely populated. At present, the statistical reliability of our constraints are limited as much by the limited survey nature of the simulations as by the small number of observed objects themselves. Continued simulation could substantial narrow the potential search area required.

As important as continued simulation, continued detection of distant solar system objects is the key to refining the orbital parameters of Planet Nine. Each addition Kuiper belt object with $a > 230$ AU tightens the observational constraints on the location of Planet Nine (or, alternatively, if significant numbers of objects are found outside of the expected cluster location, the objects can refute the presence of a Planet Nine).

Interestingly, the detection of more high semimajor axis perpendicular objects (whether Centaurs or Kuiper belt objects) has the possibility of placing the strongest constraints in the near term. While we have currently only used the *existence* of these objects as a constraint, their perihelion locations and values of ω change strongly with ω_9 and i_9 and so can be used to better refine these estimates. Though there are only currently 5 known of these objects, they are being discovered at a faster rate than the distant Kuiper belt objects, so we have hope of more discoveries soon. As with the distant Kuiper belt objects, of course, detection of these objects also has the strong possibility of entirely ruling out the existence of Planet Nine if they are not found with perihelia in the locations predicted by the hypothesis.

REFERENCES

Batygin, K. & Brown, M. E. 2016, AJ, 151, 22

Batygin, K. & Stevenson, D. J. 2013, ApJ, 769, L9

Brasser, R., Duncan, M. J., & Levison, H. F. 2006, Icarus, 184, 59

Brown, M. E. 2008, in The Solar System Beyond Neptune, ed. M. A. Barucci, H. Boehnhardt, D. P. Cruikshank, & A. Morbidelli, 335–344

Brown, M. E., Bannister, M. T., Schmidt, B. P., Drake, A. J., Djorgovski, S. G., Graham, M. J., Mahabal, A., Donalek, C., Larson, S., Christensen, E., Beshore, E., & McNaught, R. 2015, AJ, 149, 69
Brown, M. E., Trujillo, C., & Rabinowitz, D. 2004, ApJ, 617, 645
Burgdorf, M., Orton, G. S., Davis, G. R., Sidher, S. D., Feuchtgruber, H., Griffin, M. J., & Swinyard, B. M. 2003, Icarus, 164, 244
Chambers, J. E. 1999, MNRAS, 304, 793
Chen, Y.-T., Kavelaars, J. J., Gwyn, S., Ferrarese, L., Côté, P., Jordán, A., Suc, V., Cuillandre, J.-C., & Ip, W.-H. 2013, ApJ, 775, L8
Drake, A. J., Djorgovski, S. G., Mahabal, A., Beshore, E., Larson, S., Graham, M. J., Williams, R., Christensen, E., Catelan, M., Boattini, A., Gibbs, A., Hill, R., & Kowalski, R. 2009, ApJ, 696, 870
Dukes, D. & Krumholz, M. R. 2012, ApJ, 754, 56
Fienga, A., Laskar, J., Manche, H., & Gastineau, M. 2016, ArXiv e-prints
Gladman, B. & Chan, C. 2006, ApJ, 643, L135
Gomes, R. S., Matese, J. J., & Lissauer, J. J. 2006, Icarus, 184, 589
Gomes, R. S., Soares, J. S., & Brasser, R. 2015, Icarus, 258, 37
Holman, M. J., Chen, Y.-T., Lin, H.-W., Lackner, M., Payne, M. J., & Alcock, C. 2015, in AAS/Division for Planetary Sciences Meeting Abstracts, Vol. 47, AAS/Division for Planetary Sciences Meeting Abstracts, 211.12
Kenyon, S. J. & Bromley, B. C. 2004, Nature, 432, 598
Linder, E. F. & Mordasini, C. 2016, ArXiv e-prints
Luhman, K. L. 2014, ApJ, 781, 4
Malhotra, R., Volk, K., & Wang, X. 2016, ArXiv e-prints
Millis, R. L., Buie, M. W., Wasserman, L. H., Elliot, J. L., Kern, S. D., & Wagner, R. M. 2002, AJ, 123, 2083
Morbidelli, A. & Levison, H. F. 2004, AJ, 128, 2564
Petit, J.-M., Kavelaars, J. J., Gladman, B. J., Jones, R. L., Parker, J. W., Van Laerhoven, C., Nicholson, P., Mars, G., Rousselot, P., Mousis, O., Marsden, B., Bieryla, A., Taylor, M., Ashby, M. L. N., Benavidez, P., Campo Bagatin, A., & Bernabeu, G. 2011, AJ, 142, 131
Rickman, H., Froeschlé, C., Froeschlé, C., & Valsecchi, G. B. 2004, A&A, 428, 673
Rogers, L. A. 2015, ApJ, 801, 41
Smartt, S. J., Smith, K. W., Wright, D., Young, D. R., Kotak, R., Nicholl, M., Polshaw, J., Inserra, C., Chen, T.-W., Terreran, G., Gall, E., Fraser, M., McCrum, M., Valenti, S., Foley, R., Lawrence, A., Gezari, S., Burgett, W., Chambers, K., Huber, M., Kudritzki, R. P., Magnier, E., Morgan, J., Tonry, J., Sweeney, W., Stubbs, C. W. C., Kirshner, R., Metcalfe, N., & Rest, P. D. A. 2014, The Astronomer's Telegram, 5850
Trujillo, C. A. & Sheppard, S. S. 2014, Nature, 507, 471
Weiss, L. M. & Marcy, G. W. 2014, ApJ, 783, L6